



# Interfacial Fourier transform shear rheometry of complex fluid interfaces

Christopher O. Klein<sup>1,2</sup> · Antigoni Theodoratou<sup>1,3</sup> · Patrick A. Rühs<sup>4</sup> · Ulrich Jonas<sup>1,5</sup> · Benoit Loppinet<sup>1</sup> · Manfred Wilhelm<sup>2</sup> · Peter Fischer<sup>6</sup> · Jan Vermant<sup>7</sup> · Dimitris Vlassopoulos<sup>1,3</sup>

Received: 22 June 2018 / Revised: 16 November 2018 / Accepted: 25 November 2018 / Published online: 10 January 2019  
© Springer-Verlag GmbH Germany, part of Springer Nature 2019

## Abstract

Nonlinear rheometry of interfaces is very challenging because of the limits of current day instrumentation and the intricate coupling of flows at interfaces and in the bulk. The use of time periodic flows may constitute a first step in addressing this issue. Fourier transform rheology (FTR) measurements with quasi-monolayers at the air-water interface are used in order to assess the suitability of the different devices to investigate nonlinear interfacial shear viscoelasticity. The probe material was a poly (methyl methacrylate) forming a soft glassy interface, whereas complementary measurements were performed with a polystyrene latex suspension forming a predominantly viscous interface at intermediate surface coverages. The obtained data with the magnetic rod rheometer (ISR) were compared against those obtained with the bicone and the double wall ring geometries attached to standard rotational rheometers. In particular, an unexpected appearance of even in addition to odd harmonics is discussed in terms of flow field asymmetry.

**Keywords** Interfacial rheometry · PMMA · Fourier-transform-rheology · LAOS · Interfacial stress rheometer · Bowditch-Lissajous plot

## Introduction

Complex fluid-fluid interfaces can play an important role in the stabilization of heterogeneous soft materials (e.g., blends, emulsions, foams, and dispersed particulate systems) (Israelachvili

2011; de Gennes et al. 2004; de Viguerie et al. 2011; Fuller and Vermant 2011; Klein et al. 2011; Monteux et al. 2006; Russel et al. 1989; Vermant et al. 2008; Witten 2004). For example, in the case of emulsions, surfactants can stabilize the droplets of the dispersed phase due to their amphiphilic character

✉ Christopher O. Klein  
christopher.klein@kit.edu

Antigoni Theodoratou  
antigoni.theodoratou@umontpellier.fr

Patrick A. Rühs  
patrick.ruehs@mat.ethz.ch

Ulrich Jonas  
jonas@chemie.uni-siegen.de

Benoit Loppinet  
benoit@iesl.forth.gr

Manfred Wilhelm  
manfred.wilhelm@kit.edu

Peter Fischer  
peter.fischer@hest.ethz.ch

Jan Vermant  
jan.vermant@mat.ethz.ch

Dimitris Vlassopoulos  
dvllasso@iesl.forth.gr

<sup>1</sup> Foundation for Research and Technology Hellas (FORTH), Institute of Electronic Structure and Laser, P.O. Box 1527, 71110 Heraklion, Crete, Greece

<sup>2</sup> Karlsruher Institut für Technologie KIT, Institut für Technische Chemie und Polymerchemie, Engesserstr. 18, 76131 Karlsruhe, Germany

<sup>3</sup> Department of Materials Science & Technology, University of Crete, P.O.Box 2208, 71003 Heraklion, Crete, Greece

<sup>4</sup> Laboratory of Complex Materials, ETH Zurich, Vladimir-Prelog-Weg 5, 8093 Zürich, Switzerland

<sup>5</sup> Department Chemistry-Biology, Macromolecular Chemistry, University of Siegen, Adolf-Reichwein-Strasse 2, 57076 Siegen, Germany

<sup>6</sup> Institute of Food, Nutrition and Health, ETH Zurich, Schmelzbergstrasse 7, 8092 Zürich, Switzerland

<sup>7</sup> Laboratory of Soft Materials, Department of Materials, ETH Zurich, Vladimir-Prelog-Weg 5, 8093 Zürich, Switzerland

and the subsequent reduction of interfacial tension. Likewise, block copolymers act as macromolecular surfactants that stabilize polymer blends (Macosko et al. 1996). It is also known that particles can accumulate at the interface (Binks and Horozov 2006; Binks 2002; Fischer and Erni 2007; Leal-Calderon and Schmitt 2008; Murray 2002; Stocco et al. 2011; Vermant et al. 2008; Xu et al. 2007) in Pickering emulsions and these modify the interfacial mechanics more than they affect interfacial tension (Thijssen and Vermant 2018). Biofilms at interfaces have received a great deal of attention because of their numerous applications in medical and environmental fields (Hollenbeck et al. 2014; Rühls et al. 2013a,b; Wu et al. 2012), and interfacial rheology is of interest as the interactions between the bacteria can be measured without interference of the interactions with the substrate.

Understanding the dynamics and the mechanical properties of interfacial layers is of scientific and technological relevance (Erni and Parker 2012; Fuller and Vermant 2012; Sagis 2011; Sagis and Fischer 2014; Reinheimer et al. 2011). The interfacial rheological material functions can be used to rationally design interfaces for specific target applications. Concerning planar liquid interfaces, significant progress has been made recently in the development of experimental tools to measure their linear viscoelastic properties (Gordon 1986; Brooks 1999; Brooks et al. 1999; Choi et al. 2011; Erni et al. 2003; Fuller 2003; Reynaert et al. 2008; Rühls et al. 2012; Vandebril et al. 2010). To date, three state-of-the-art experimental setups that are readily available are (i) the bicone fixture (Erni et al. 2003) and (ii) the double wall ring (DWR), both connected to a rotational rheometer (Vandebril et al. 2010), as well as (iii) the magnetic-rod interfacial stress rheometer (Gordon 1986; Brooks et al. 1999; Verwijlen et al. 2011). On the other hand, there are only a few studies on nonlinear interfacial rheology (Danov et al. 2012; Erni et al. 2012; Erni and Parker 2012; Hyun et al. 2011; Jaishankar et al. 2011; Krishnaswamy et al. 2007; Sagis and Fischer 2014; Torcello-Gomez et al. 2011; Zang et al. 2010). For shear rheometry, such experiments were typically conducted by using the special fixtures adapted to commercial rheometers, i.e. the bicone geometry (Torcello-Gomez et al. 2011; van den Berg et al. 2018), or the DWR (Hermans and Vermant 2014; Samaniuk and Vermant 2014; Theodoratou et al. 2016). For the magnetic rod-based interfacial stress rheometer (ISR), which is the most sensitive device (Brooks et al. 1999; Reynaert et al. 2008; Verwijlen et al. 2011), nonlinear measurements have not yet been reported.

An important aspect in interfacial rheology is the unavoidable hydrodynamic coupling between bulk and interfacial flows. The drag exerted by the flow in the surrounding bulk phases directly contributes to the total drag force on the measurement probe, in addition to the surface drag. Moreover, through the effect of bulk dissipation of momentum on the interfacial velocity profile, the interfacial velocity profile depends on the extent of this coupling. The shear rate at the edge

of the measurement geometry is hence not given by the value expected from a linear velocity profile, but it will be strongly enhanced, in particular for smaller values of the interfacial material functions. The importance of bulk relative to interfacial flows is quantified by a dimensionless group, the Boussinesq number. To obtain the correct shear rate at the measurement probes, iterative solution procedures have been designed for the magnetic rod rheometer (Reynaert et al. 2008; Verwijlen et al. 2011; Fitzgibbon et al. 2014; Tajuelo et al. 2016), the DWR (Vandebril et al. 2010), and the bicone (Fischer and Erni 2007; Tajuelo et al. 2018) setups. With these corrections, linear viscoelastic material functions can be determined in oscillatory shear flows. For knife edge viscometers, such analysis has been also implemented for a range of steady-state surface viscosities (Raghunandan et al. 2015; Lopez and Hirs 2015) and recently for the more complicated case of a steady-state non-Newtonian surface viscosities (Underhill et al. 2017). It has been shown using direct visualization methods that the nonlinear response regime in steady-state flow far into the nonlinear regime is often characterized by inhomogeneous deformations at the interface (Barman and Christopher 2014). The nonlinear boundary condition set by the nonlinear rheological response makes the already non-linear problem of coupling between bulk and interfaces even more strongly nonlinear.

For bulk systems, a wide range of nonlinear test protocols is available. Recently, large amplitude oscillatory shear (LAOS) rheometry has been proposed as an easy to perform but difficult to analyze method, which minimally gives a “fingerprint” of the onset of nonlinear response and as such has been used for a range of soft matter systems, such as polymer melts, polymer solutions, food grade biopolymers, proteins, and colloidal materials (Fardin et al. 2014; Cho et al. 2005; Fischer and Erni 2007; Hyun and Wilhelm 2009; Hyun et al. 2011; Wilhelm 2002; Wilhelm et al. 1998; Singh et al. 2018; Rogers 2018). It represents a gentle way to enter the nonlinear deformation regime. During a LAOS experiment, a sinusoidal strain or stress is applied to the sample. In the linear regime, the sample responds with a stress or strain signal of the same frequency but different amplitude and phase depending on its viscoelasticity, whereas in the nonlinear regime, the response signal consists of higher harmonics at multiples of the excitation frequency,  $\omega = f/2\pi$  (in Hz). In contrast to linear viscoelastic properties, nonlinear response functions feature distorted (but periodically self-repeating) oscillatory wave shapes, which are analyzed by either Fourier transform rheology (FTR) or by Bowditch-Lissajous curves. In FTR, the nonlinear mechanical behavior is captured by the presence of higher harmonics (at  $3\omega_1$ ,  $5\omega_1$  etc) in a periodic response signal under oscillatory shear (Hyun et al. 2011; Rogers et al. 2011). The nonlinearity is then quantified in FTR via the intensities and the phases of the higher harmonics. The LAOS response can also be described by the so-called Bowditch-Lissajous curves (Ewoldt and Bharadwaj 2013;

Klein et al. 2007; Wilhelm et al. 2012; Rogers et al. 2011) where stress is plotted versus strain or strain rate. Recent improvements of the LAOS response aiming at some physical interpretation of the nonlinear response signals include the geometric stress decomposition (Cho et al. 2005) and the use of Chebychev polynomials (Hyun et al. 2011; van Dusschoten and Wilhelm 2001), the sequence of physical processes (Rogers 2012; Rogers et al. 2011) and rescaling the dependence of the higher harmonics on the strain amplitude (Hyun and Wilhelm 2009).

In light of the above, as well as the occurrence of large nonlinearities during the deformation of drops and bubbles, it is highly desirable to obtain better understanding of both the linear and the nonlinear response of molecules or particles at fluid interfaces (de Viguier et al. 2011; Ermi and Parker 2012; Klein et al. 2011; Reynaert et al. 2008; Sagis and Fischer 2014; Vandebril et al. 2010). In analogy to bulk LAOS, we propose to use time periodic flows as a first step in addressing the issue of nonlinear interfacial response, using the fingerprint embedded in the higher harmonics of the stress or strain response to evaluate the performance of the different instruments as well as the intrinsic responses. First, the magnetic-rod ISR designed by Brooks et al. (1999) was adapted to measure nonlinear rheological response using FTR methodology and analyze the recorded response signal for higher harmonics of the frequency. The ISR is a stress-controlled rheometer where the motion of the magnetic probe is measured with an optical encoder, similar to strain measurements in the bulk rheometers. To be able to use the FTR methodology, the ISR was calibrated in such a way that for a given magnetic force field a known deformation could be achieved. The accessible range of excitation amplitudes and frequencies within a linear subphase response, as well as technical limitations inherent in the current setup, were established and analyzed. An advantage of the FTR implementation is that it increases the measurement range and the accuracy for viscous and viscoelastic interfaces (van Dusschoten and Wilhelm 2001). While controlling the surface at a constant value, a magnetic rod was displaced in a sinusoidal way parallel to the air-water interface, resulting in a shear deformation of the interface. The same sample film can be measured at different surface pressures. Surprisingly, a second harmonic was always detected in the ISR. The FTR analysis of LAOS signals in bulk systems may sometimes yield even harmonics, which are associated with wall slip (Hyun et al. 2011). To explore the origin of the 2nd harmonics, a protocol was implemented, involving tests with different systems (polymeric and a colloidal particle quasi-monolayers at the air-water interface) and geometries (different types of rods, different channel width, channel with grafted inner walls), as well as complementary tests with the bicone and DWR setups mounted on commercial rheometers.

Simple shear deformations have the advantage that the mechanical response is interrogated at constant surface

area, and only the deviatoric contributions to the interfacial and bulk stress are measured. Nonlinear rheometry using more complicated deformations, for example using a Langmuir trough with oscillating barriers (Brooks et al. 1999) or oscillating pendant or sessile drops (Fischer et al. 2000; Hilles et al. 2006; Kralchevsky and Nagayama 1994; Sagis and Fischer 2014; Kotula and Anna 2015) have two major complications. First, there is an interplay between changes in surface concentration and its effect on surface pressure (compressibility of the layers) and the surface rheology. Second, these instruments all have complex mixed shear/dilation deformation modes making the analysis rather cumbersome (Pepicelli et al. 2017, Nagel et al. 2017). For more details, we refer to a recent review by Jaensson and Vermant (2018).

The present work aims to investigate if the nonlinear response of interfaces can indeed be characterized by the rheological LAOS “fingerprinting technique” and how the different devices for shear rheometry respond to large interfacial shear deformations. The paper is organized as follows: after this introduction, the experimental systems and setup are presented in section “Experimental”. The results for both polymeric and colloidal interfaces are the subject of section “Experimental results”. In section “Discussion of issues associated with measurements using the magnetic-rod ISR”, we analyze and discuss the results, and finally, the main conclusions are summarized in the last section.

## Experimental

### Materials

All materials were used as received, unless stated otherwise. Ultrapure water with a resistivity of 18.2 M $\Omega$ cm was obtained with a Millipore water system ion exchange, UV-irradiation, and filtration steps and used as subphase in the Langmuir trough.

The poly (methyl methacrylate) (PMMA) sample was obtained from PSS (Mainz, Germany) and was synthesized by anionic polymerization. It had a weight-average molar mass of 270,000 g/mol and a molar mass dispersity  $M_w/M_n = 1.04$  (with the subscripts w and n denoting the weight- and number-average molar masses, respectively). An amount of 30 mg was dissolved in 30 mL of chloroform, a good solvent for PMMA. Surface deposition of the polymer solution at the air-water interface was performed by spreading the solution drop by drop with a 20- $\mu$ L syringe. The polymer layer was left at rest for about 15 min to allow a complete evaporation of the solvent.

Colloidal polystyrene latex particles were prepared by surfactant-free emulsion polymerization, using about 1% wt. acrylic acid as co-monomer during the polymerization, leading to spherical particles with an average diameter of 538 nm  $\pm$  21 nm (Retsch et al. 2009). The solid content of

the final emulsion was 2.0 wt% as determined gravimetrically. The obtained aqueous dispersion was purified by several cycles of centrifugation and re-dispersion in water, yielding the stock suspension. In order to remove amphiphilic polymer fractions (from the emulsion polymerization process) physisorbed at the particle surface, the latex suspension was mixed with ethanol (1:5 volume ratio), centrifuged, and the supernatant replaced by pure ethanol. The particles were then re-dispersed using ultrasonication. This procedure was repeated five times, and then, the final suspension was kept in ethanol. Both the “raw” and the “ethanol-washed” suspensions were investigated. The latter was spread directly from the ethanol dispersion, whereas the former was spread after dilution in ethanol (1:5 volume ratio). Surface deposition of the colloidal particles at the air-water interface was performed by spreading the particle suspension drop by drop with a 5-mL pipette.

## Apparatuses and procedures

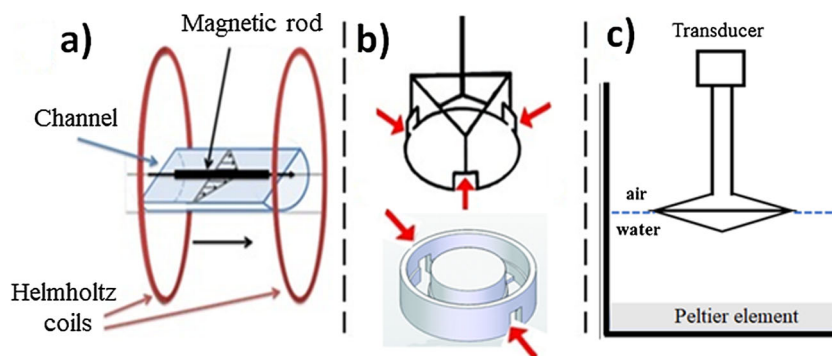
### Interfacial shear rheometer (ISR)

The experimental setup consisted of a commercial Langmuir trough coupled with a magnetic rod interfacial stress rheometer (ISR) from KSV Instruments, Finland (Minitrough 4 with ISR 400) (Brooks et al. 1999). A Wilhelmy-plate (platinum) coupled to an electromagnetic balance was half immersed into the water phase and oriented parallel to the direction of the barrier motion in order to monitor the surface pressure. The temperature was stabilized at  $25.0 \pm 0.5$  °C by means of a recirculating water/ethylene glycol bath. For the rheological measurements, a rheological probe (magnetic rod) was positioned at the water-air interface in a flow channel and oriented with the long axis parallel to a homogeneous magnetic field (see Fig. 1a). A periodic oscillatory modulation in the magnetic field induced an oscillating movement of the magnetic rod in the direction of the long axis, in the plane of the water-air interface. The maximum field strength was  $2.0 \times 10^{-3}$  T, and the resulting forces that could be applied range from  $10^{-3}$  to 30  $\mu$ N (Brooks et al. 1999). The oscillatory movement of the magnetic rod sheared the interfacial layer

sinusoidally within the channel. The position of the magnetic rod was optically detected with a camera (Sony XC-HR50, lens from Edmund Optics, UK). More specifically, the edge of one end of the rod was monitored, and the position was recorded in pixels of the camera. With an excitation frequency  $\omega$  ranging from 0.0016 to 4 Hz, and a strain amplitude  $\gamma_0$  ranging from 0.1 to 100% (equaling half the width of the channel). The interfacial storage modulus  $G^{s'}$  and the interfacial loss modulus  $G^{s''}$  were measured with a resolution of about  $\pm 1$   $\mu$ N/m.

**Magnetic rods and channels** In order to test the possibility of wall slip, different combinations of probes and channels were used: (i) a Teflon-coated steel sewing needle that can be approximated as a rod with length 55.2 mm and diameter of 500  $\mu$ m (Brooks et al. 1999); (ii) a glass capillary with an embedded magnetic rod in the center (Reynaert et al. 2008). It had a length of 41 mm and a diameter of 400  $\mu$ m. It is important to note that, unlike the glass rods, the Teflon-coated sewing needles were not fully symmetric but had one sharp and one blunt tip; (iii) in order to optimize the interaction between the surface of the glass capillary rod and the interface in the case of the polymeric layer, PMMA was grafted onto the glass capillary surface. The grafting procedure involved the following steps. The surface of the rod was first cleaned, by immersing it for 3 h in a 2% v/v alkaline Hellmanex solution (Hellma-Analytics, Germany). Subsequent cleaning steps included rinsing with water and ethanol, followed by drying first under nitrogen atmosphere and then using vacuum at room temperature. Afterwards, the glass rod was immersed overnight in a 4-benzoylphenoxypropyl-(triethoxy) silane ethanol solution, followed by further cleaning with ethanol in order to remove the unreacted silane and then drying in nitrogen. PMMA was adsorbed by dipping the rod in a 2% w/w PMMA solution in THF. The rod coated with the PMMA film was dried for about 12 h and then irradiated with UV light (wavelength 365 nm) for about 30 min in order to graft the PMMA into the surface. Ungrafted polymer was washed away with a THF solution (Prucker et al. 1999). (iv) Polyoxymethylene (POM) channels were used with width of 9 or 7 mm to test for possible width dependence of viscoelastic properties and a length of 90 mm. To further enhance the contact between the floating PMMA layer

**Fig. 1** Sketch of the rheometric setups, including (a) the ISR with the magnetic coils, the flow Channel, and the magnetic rod; (b) the DWR (double wall ring) fixture with its cup; and (c) the bicone geometry





and the channel walls, one channel was grafted with PMMA following the abovementioned procedure. In all experiments with the ISR, we followed the same procedure for rod magnetization. As in all experiments with the PMMA in the different instruments, the Bousinesq numbers were high; hence, only linear corrections needed to be applied in order to correct for the instrument contribution (for example, for the PMMA layers at 0.1 Hz, the values amounted to 89,000, 119,000, and 17,000 for ISR, DWR, and bicone setups, respectively).

**Signal analysis** To use the ISR for nonlinear rheological measurements, the measurement and control software had to be adapted. The frame rate of the camera was 30 fps, limiting the time resolution to about 33 ms. This sampling rate is relevant for the frequency of the modulation signal of the magnetic field and for the detection of the movement of the magnetic rod. Accordingly, a user-defined oversampling (van Dusschoten and Wilhelm 2001) of both the optical data and the command voltage for generating the magnetic field was integrated into the ISR acquisition software using Labview. At sufficiently slow excitation frequencies, oversampling takes averages over longer acquisition times, and therefore substantially reduces the stochastic noise in the data. Averaging is only done if the time resolution of the data acquisition is sufficient to detect the desired highest frequency of the measurement. This highest detectable frequency is set by the Nyquist frequency. It is defined as half the sampling frequency of a discrete signal,  $\omega_{\max} = 1/2t_{\text{DW}}$  (where  $t_{\text{DW}}$  is the dwell time) (Grenander 1959). With a maximum time resolution of 30 Hz ( $t_{\text{DW}} = 33$  ms), the Nyquist frequency is 15 Hz. As a consequence for the present setup, if the magnetic rod of the ISR is excited with a maximum frequency of 1 Hz, and without using oversampling, the detection limit is the 15th higher harmonic. For higher frequencies, oversampling should not be conducted, because it would reduce the amount of data points per second by averaging to a value that is not sufficient anymore to resolve potential higher harmonics, therefore resulting in unreliable data. For frequencies below 1 Hz, oversampling was applied, resulting in a better signal-to-noise ratio of the raw data. Nevertheless, the present setup demonstrates a proof of concept. The current limitations may be overcome by using higher-speed cameras.

### Bicone geometry

Complementary experiments were performed using a standard rotational rheometer (MCR 501, Anton Paar, Austria) with a bicone geometry (Erni et al. 2003). The bicone geometry is oscillating or rotating with a controlled torque or strain. The cup remains stationary and the disk oscillates. The cup inner radius is 40 mm, the disk radius is 34.14 mm, and the cone angle is  $5^\circ$  (see Fig. 1c).

### Double wall ring geometry

A stress-controlled DHR-3 rheometer (TA Instruments, USA) was also used in conjunction with a double wall ring geometry and a Langmuir trough (Vandebril et al. 2010; Hermans and Vermant 2014). The sample is contained in a trough and the DWR geometry is positioned in an open Teflon cup connected to a temperature-controlled Langmuir trough. The ring is made from titanium (Ti6Al4V Grade 5); its inner diameter is 34 mm and its outer diameter is 36 mm. Openings in the ring and cup allow for the surface pressure to be regulated (see Fig. 1b).

## Experimental results

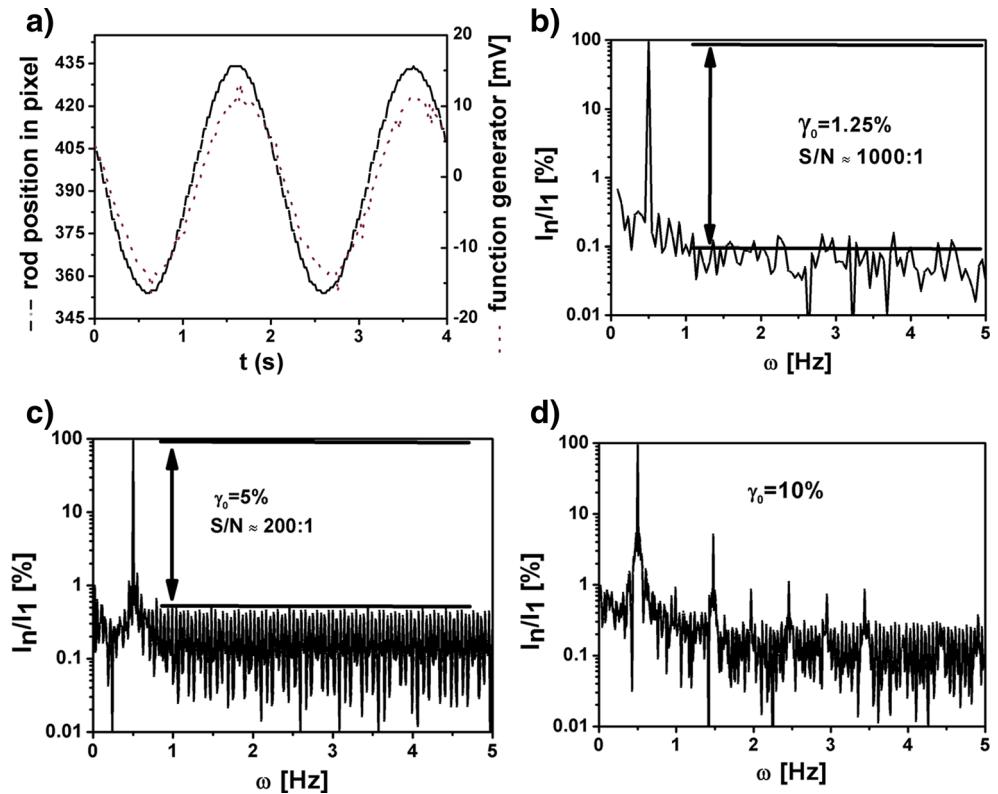
### Reference state: the subphase response in ISR

Since water is the common subphase in all experiments, its response was measured and analyzed (without any sample layer) with the adapted ISR software and FT. We performed this reference test with the Teflon-coated magnetic rod, which is the main probe rod used, and only compared the responses of different rods at colloidal and polymeric interfaces. In order to determine the linear regime of the pristine water subphase, the quality of the excitation and response signal in the frequency range  $\omega = 0.01$ –4 Hz was investigated. The lower frequency limit was determined by the digitization limits of the camera setup being able to resolve the strains. The upper limit was set by the magnetic rod's motion deviating from a linear one and becoming erratic (as discussed below).

Figure 2a displays the time-domain signal of the water subphase, for both the excitation and response. The related magnitude spectrum of the Fourier transform of the excitation signal is shown in Fig. 2b for a strain amplitude of 1.25%. The response signal has a typical signal-to-noise (S/N) ratio of 1000:1 for the first harmonic, and no higher harmonics indicative of nonlinearities are discernible. The time resolution is sufficient to detect potential nonlinearities in a frequency range up to 1 Hz.

The frequency domain data of the response for the pure water subphase is shown for two additional strain amplitudes of  $\gamma_0 = 5\%$  (Fig. 2c) and  $10\%$  (Fig. 2d). At  $\gamma_0 = 5\%$ , only the first harmonic is seen, and Fig. 2c indicates a S/N ratio for the first harmonic of about 200:1. When increasing the strain amplitude to  $\gamma_0 = 10\%$ , the water signal does contain higher harmonics (Fig. 2d) due to nonlinear mechanical response. Note, however, that for  $\omega = 4$  Hz, the effective Reynolds number is  $Re = \rho a^2 / \eta \approx 0.25$  (with  $a$  the rod radius); hence, inertial effects could start to play a role. The higher harmonics could also originate from an irregular movement at large displacements of the magnetic rod, which resides inside a channel that is only slightly longer than the rod. The water meniscus inside

**Fig. 2** Time (a) and frequency (b) domain data of the excitation (a function generator) and response (b position) signal of the ISR at  $\omega = 0.5$  Hz. The signal-to-noise ratio of the first harmonic is 1000:1 at a strain amplitude of  $\gamma_0 = 1.25\%$ . (c) Magnitude spectra of the response signal from the pristine water subphase at a strain amplitude  $\gamma_0$  of 5% and (d) 10%

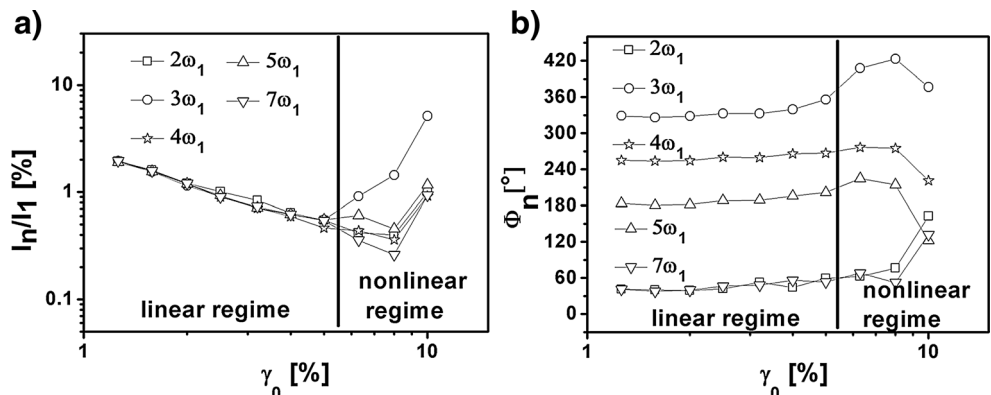


the hydrophilic channel is concave and the magnetic rod lies with its long axis parallel to the channel axis in the minimum of the concave meniscus due to gravitational forces acting on the rod. During large-amplitude oscillations of the rod, the tip approaches the end of the channel where the shape of the water surface is not concave anymore. The magnetic rod may perform slightly irregular motion (not necessarily visible by the camera), yielding higher harmonics. Another possible effect is the non-symmetric shape of the metallic rod used in these experiments (see also section “Interfacial shear rheometer”), as the needle has two different edges, one sharp and one blunt (Brooks et al. 1999). However, the compressibility of the interface should smooth out possible local divergence of the flow; hence, the effects of the asymmetry of the magnetic rod on the flow field should be very small. This is indirectly

confirmed here since more regular glass capillary rods have been used as well, and the effects vis a vis appearance of even harmonics are similar, as discussed below.

In Fig. 3, the results from the analysis of the response of the water subphase are presented in the form of (a) normalized intensity and (b) the phases of the higher harmonics, both as functions of the strain amplitude. In the range of  $\gamma_0 = 1.2\text{--}5\%$  (Fig. 3a), a slightly negative slope is observed. When looking at the magnitude spectra of Fig. 2c, it becomes clear that the  $I_n/I_1$  values at the frequencies corresponding to the position of higher harmonics do not originate from nonlinearities in the sample, but from the ratio of the first harmonic to the background noise level. As the strain amplitude increases, the detected stress is enhanced,  $I_1$  as absolute value is increasing, while the noise level remains constant in absolute value.

**Fig. 3** Normalized amplitudes  $I_n/I_1$  (a) and phases  $\Phi_n$  (b) of the higher harmonics of the response (strain) signals of the neat water subphase. The excitation frequency was  $\omega = 0.5$  Hz. Error bars are within the size of the symbols. Channel width 9 mm, Teflon-coated steel rod (see section “Interfacial shear rheometer”). The linear regime is dominated by noise



Consequently,  $I_n/I_1$  then scales with  $\gamma_0^{-1}$  if a constant noise level is assumed. These measurements are therefore still considered to be in the linear regime, albeit dominated by noise. When increasing the strain amplitude above  $\gamma_0 = 5\%$ , the non-linear response from the subphase is larger than the noise of the apparatus and therefore an onset and the intensity increase of the higher harmonics can be detected. Within the FTR spectrum, the 3rd harmonic is the most prominent of the higher harmonics (Fig. 3a). An increase of the signal-to-noise ratio at very large amplitudes apparently results most likely from a wiggling motion of the magnetic rod at large displacements, as discussed above. In order to overcome this amplitude limitation, potentially the channel length could be increased.

Next, the frequency-dependent phase spectra of the strain response (Fig. 3b) are considered, which should always be interpreted together with the magnitude data. In analogy to the normalized intensities of the harmonics, for strain amplitudes  $\gamma_0 > 5\%$ , the phase angle of the higher harmonics starts to vary substantially. Note that, in general as the phase of the higher harmonics  $\Phi_n$  is very sensitive to variations in the mechanical behavior, a stable phase  $\Phi_n$  serves as a necessary experimental condition for a stable, reproducible signal.

As a consequence of the above observations, reliable rheological measurements on interfacial layers without nonlinear contributions of the water subphase can be performed up to a strain amplitude of  $\gamma_0 = 5\%$  with the present setup. Water can be used as standard (reference) subphase in the Langmuir trough for the FT-ISR measurements.

### Polymeric (PMMA) quasi-monolayers: surface pressure isotherms, linear viscoelasticity, and FTR analysis with the ISR

**Surface pressure isotherms** Given the ability of PMMA to form macroscopically homogeneous and insoluble layers at the air-water interface (Srivastava et al. 2011), arising from the presence of a polar group (carboxy ester), it is a promising candidate for investigating the respective rheological nonlinearities. After spreading, a compression and expansion cycle with a speed of 50 mm/min was performed with a final compression up to the desired final surface pressure of  $20 \text{ mN m}^{-1}$ , followed by a rest time of 15 min, needed to create a homogeneous layer in the channel. Whereas bulk PMMA has a high glass transition temperature  $T_g$  (of about  $115 \text{ }^\circ\text{C}$ ), it is plasticized at the air-water interface (Fujii et al. 2010; Hancock and Zografis 1994; Kim et al. 2017; Witte et al. 2010). If we used the estimated radius of gyration of about 11 nm (Rubinstein and Colby 2003) as a typical distance from the interface (with water), the  $T_g$  should be around  $67 \text{ }^\circ\text{C}$  based on literature evidence (Fujii et al. 2010). This suggests that despite plasticization, the films are expected to show glassy behavior, as shown recently (Srivastava et al. 2011). Here, we are interested in the analysis

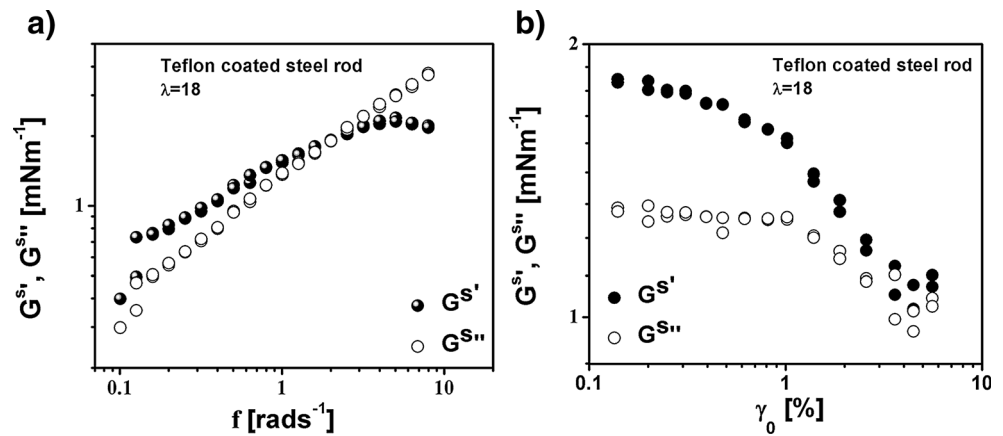
of the strong viscoelastic signal coming from the PMMA interface and do not consider their microscopic details further.

**Linear viscoelasticity** Oscillatory measurements on the PMMA quasi-monolayers were performed at  $25 \text{ }^\circ\text{C}$  (Fig. 4). For these experiments, a surface pressure of  $16 \text{ mN m}^{-1}$  was chosen, since the magnetic rod could still easily deform the polymer quasi-monolayer. In Fig. 4, data from a dynamic frequency sweep ( $\gamma_0 = 0.1\%$ ) (Fig. 4a) and a dynamic strain amplitude sweep (Fig. 4b) are depicted, employing a Teflon-coated steel rod and a channel with length, normalized by the rod diameter of  $\lambda = 18$ . The PMMA quasi-monolayer exhibits an elastic behavior with the storage interfacial modulus being slightly larger than the loss interfacial modulus up to  $f = 2 \text{ rad/s}$  (Fig. 4a). In the limited frequency range available,  $G^{sr}$  exhibits a power-law dependence on frequency with an approximate slope of 0.5 whereas the respective slope of  $G^{sm}$  approaches 1. In Fig. 4b, the oscillatory strain sweep data are depicted at  $\omega = 0.1 \text{ Hz}$  showing dominant elastic properties up to  $\gamma_0 = 5\%$  and a linear regime up to  $\gamma_0 = 0.3\%$ .

**FTR analysis** The same surface pressure of  $16 \text{ mN m}^{-1}$  was used. The frequency domain data, i.e., magnitude spectra and phase spectra of the LAOS experiments of the PMMA quasi-monolayer with the Teflon-coated steel rod, are presented in Fig. 5. The intensity of the higher harmonics increases with strain amplitude. A remarkable feature is the high intensity of the second harmonic. The second harmonic becomes significant and reaches a magnitude exceeding the 20% of the first harmonic ( $I_{2/1} \approx 20\%$ ), whereas for the third  $I_{3/1} > 10\%$ . In the phase information of Fig. 5b, the values of the 2nd and the 3rd harmonics change only slightly with increasing  $\gamma_0$ . This stability of the values of the phases of the harmonics indicates a stable and reproducible signal.

**Bowditch-Lissajous representation** It is possible to analyze nonlinear rheological behavior by means of Bowditch-Lissajous plots, where the strain is plotted against the stress (Fig. 6). The data at  $\gamma_0 = 0.4\%$  (Fig. 6a) correspond to the linear response, whereas at  $1\%$  (Fig. 6b) and at  $5.6\%$  (Fig. 6c), an increasingly clear nonlinear response is observed. At  $\gamma_0 = 0.4\%$ , some distortion of the plots is observed, most probably related to the digitization of the motion by the camera. Nevertheless, the shape of the curve is consistent with a viscoelastic solid response, expected for a glassy polymer layer. While the shape of the Bowditch-Lissajous plots at  $\gamma_0 = 1\%$  (Fig. 6b) is still consistent with linear behavior, the plot at  $\gamma_0 = 5.6\%$  (Fig. 6c) clearly departs from an elliptical shape and exhibits a weak time evolution, indicating a deformation-dependent material response. This specific time evolution could be attributed to issues associated with the choice of the rod and channel, as discussed in section “Reference state: the subphase response in ISR”, although intrinsic hysteresis cannot be excluded in this

**Fig. 4** Frequency and strain amplitude sweep for a PMMA layer at the air-water interface. The interfacial storage modulus,  $G^{s'}$  (black symbols) and the interfacial loss modulus  $G^{s''}$  (open symbols) are depicted as functions of (a) frequency ( $\gamma_0 = 0.1\%$ ) or (b) strain amplitude ( $\omega = 0.1$  Hz) (surface pressure = 16 mN/m, surface concentration = 0.47 mg/m<sup>2</sup>,  $T = 25$  °C, Teflon-coated steel rod,  $\lambda = 18$ .)



glassy system. Note that interfacial tension could also affect the position of the magnetic rod at the interface since, due to the compression, the surface tension increases and consequently the contact angle between the water phase and the rod decreases. Moreover, the use of a PMMA-grafted rod likely promotes the microscale heterogeneity of the measuring system due to the same glassy response issues associated with glassy PMMA and plasticization, as discussed above for the PMMA quasi-monolayers (Kim et al. 2017; Fujii et al. 2010). Nevertheless, the important result here is the sensitivity of the Bowditch-Lissajous plots to the transition from linear to non-linear interfacial rheological response.

**Inertial, geometric, and flow asymmetry issues** The effects of different potential contributions to the nonlinear signal, such as subphase inertia, rod/channel sizes, and symmetry, have been already discussed in section “Reference state: the subphase response in ISR”. Here, we focus on the appearance of even harmonics and in particular on the second harmonic, for different combinations of rods and channels. In Fig. 7a, the FT magnitude spectra of PMMA quasi-monolayer are presented for  $\gamma_0 = 1\%$  (aspect ratio of channel width to Teflon-coated steel rod diameter  $\lambda = 18$ ) where we observe the presence of 2nd harmonics. These results serve as reference for the subsequent comparisons. The inset of this figure shows the

normalized intensity of the 2nd harmonic as a function of imposed strain amplitude. Whereas the effects of rod asymmetry are not expected to be significant for compressible layers as already mentioned, we compare here FTR results with different combinations of rods and channels. Figure 7b depicts data taken with the same Teflon-coated steel rod used in Fig. 7a, but with a different channel having a width of 7 mm ( $\lambda = 14$ ). We observe again the presence of the 2nd harmonics, whose intensity is increasing by increasing strain amplitude (inset). Comparing the normalized amplitudes of 2nd harmonics for the two channels (insets of Fig. 7a, b), we note a different behavior when the width of the channel is altered: by employing a narrower channel, we obtain a monotonically increasing amplitude of the 2nd harmonic as function of the strain amplitude, while a more irregular dependence is obtained for the wider channel.

To evaluate the effect of nonzero Reynolds number, we increased the subphase viscosity by factor of 10 via mixing water with glycerol (56% glycerol v/v), leading to a tenfold decrease of the Reynolds number. The relevant experimental results with the Teflon-coated steel rod are depicted in Fig. 7c. We observe a very similar response when comparing with Fig. 7a, b, vis a vis the presence of 2nd harmonics. In particular, comparing Fig. 7b, c with the same  $\lambda = 14$ , we note that the normalized 2nd harmonics are virtually the same. Hence,

**Fig. 5** FTR data: magnitudes (a) and phases (b) of the 2nd, 3rd, 5th, and 7th harmonics for the PMMA layer. The measurements were performed at a surface pressure of 16 mN m<sup>-1</sup>. The excitation frequency was  $\omega = 0.1$  Hz. The error bars are within the size of the symbols

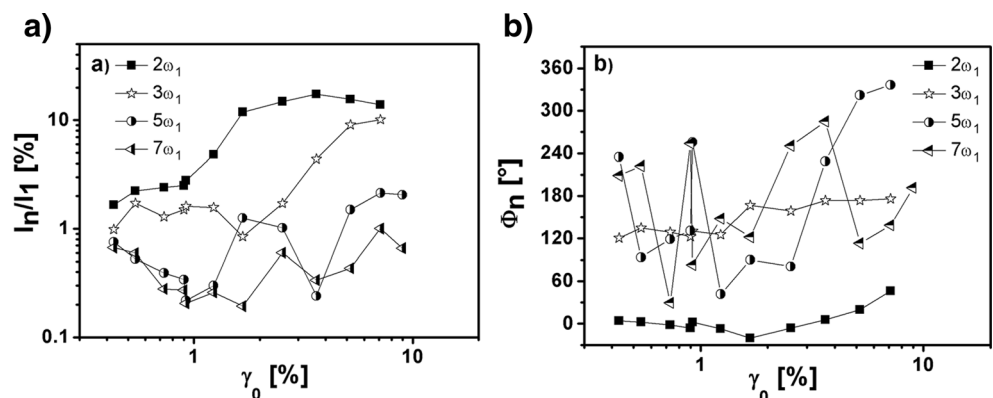
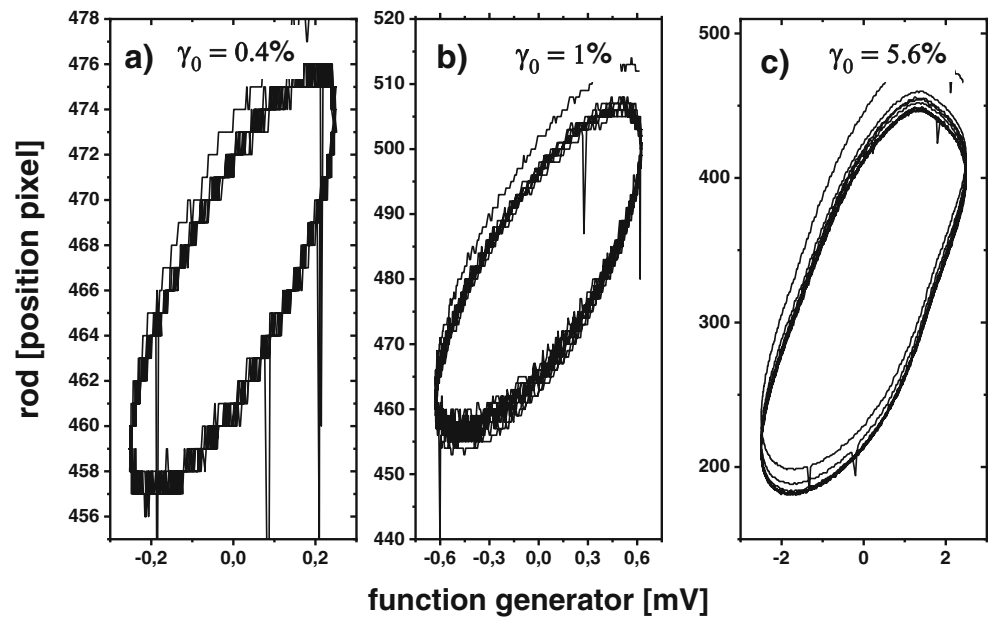




**Fig. 6** Bowditch-Lissajous plots of the LAOS data obtained with the PMMA quasi-monolayer (Fig. 6) at strain amplitudes of (a)  $\gamma_0 = 0.4\%$ , (b)  $\gamma_0 = 1\%$ , (c)  $\gamma_0 = 5.6\%$ . Plotted here is the rod position in pixel as stress against the function generator in mV as excitation signal. The excitation frequency was  $\omega = 0.1$  Hz, the Teflon-coated needle with  $\lambda = 18$  was used at a surface pressure 12 mN/m



inertial effects do not seem responsible for the appearance of the 2nd harmonic. Furthermore, we employed the same Teflon-coated steel rod in conjunction with a PMMA-coated POM channel (Fig. 7d) with the thought of possibly improving the contact between the PMMA layer and the walls of the channel, even if this is not guaranteed because of the abovementioned glassy nature of PMMA at room temperature. We also tested a PMMA-grafted glass rod (Fig. 7e), facing, however, the same issues. Finally, the effect of rotating the channel with respect to the magnetic field's lines to make flow and magnetic field non-coaxial was examined as well, using a Teflon-coated steel rod (Fig. 7f). In all cases, we detect even harmonics, with virtually the same normalized values of the second harmonic (insets). It is therefore confirmed that even harmonics are always present, over the entire strain amplitude range investigated. We conclude that upon changing the width of the rod and the surface chemistry of both the rods and the channels, we do not suppress even harmonics; hence, we cannot attribute their occurrence to these features.

In Fig. 7g, the phases of the 2nd harmonics ( $\Phi_2$ ) are presented as a function of the strain amplitude for all the investigated cases using the magnetic-rod ISR. Using the channel with  $\lambda = 14$  (filled squares) and the same channel but non-coaxial field and flow lines (open triangles), the phase of the 2nd harmonics is constant, indicating a strong and reproducible signal. With the PMMA-grafted rod (open squares), an increase of the 2nd harmonic phase is detected. It is worth to mention here that the phases discontinuously jump from 0 to  $360^\circ$  and vice versa due to the phase periodicity. For this reason, few data points have been corrected by adding  $360^\circ$ . Following Klein (2005), we have plotted the data in the phase range between 0 and  $720^\circ$ . Looking at the case with  $\lambda = 14$  (filled squares), the signal starts to be stable for strain amplitudes higher than  $\gamma_0 = 5\%$ . Interestingly, a rapid fall is

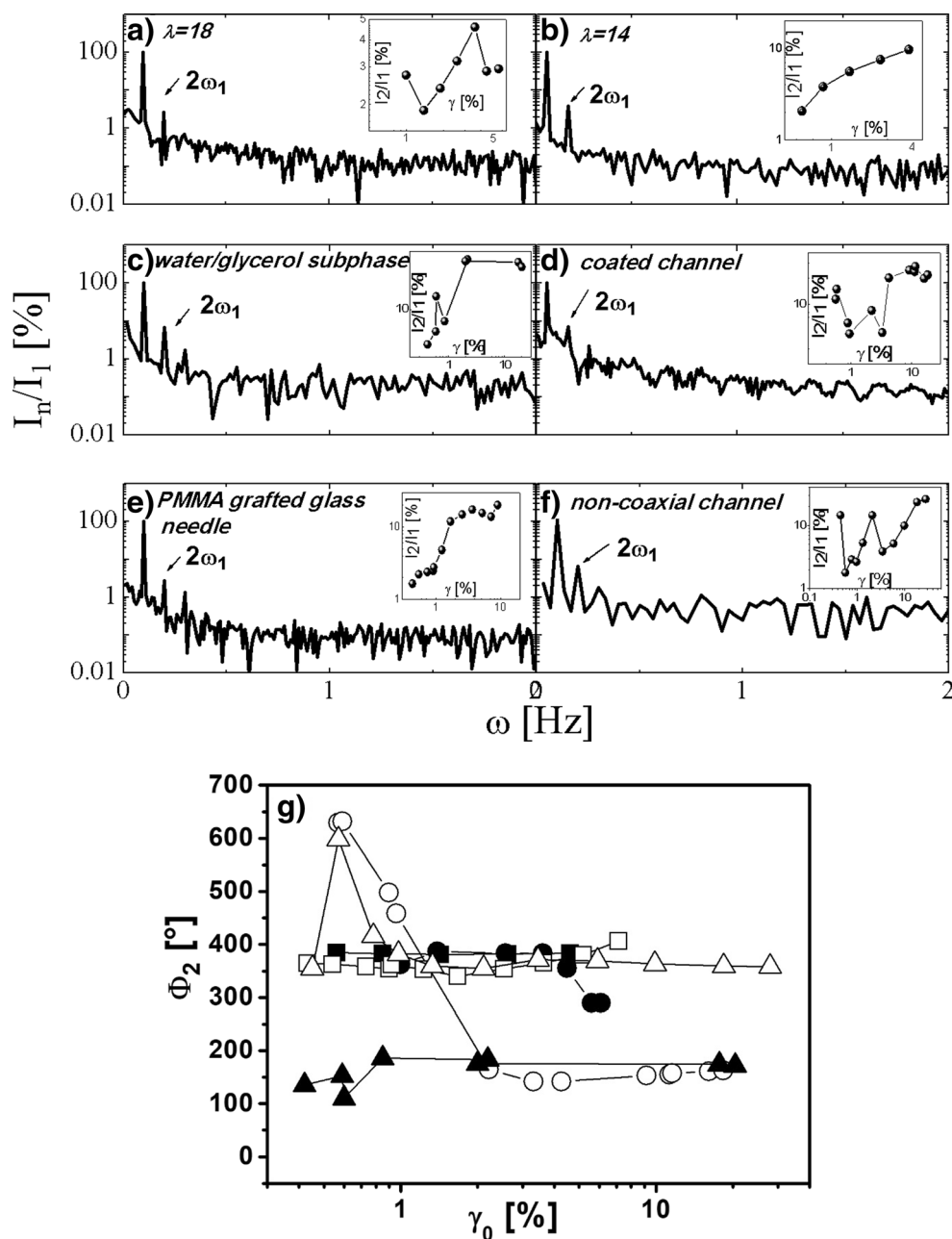
observed for the case of the PMMA-grafted channel (open circles) that we attribute to the low and unstable amplitude. The intensities and the phases of the 2nd harmonic are strain-dependent and less reliable, while the other methods give strain-independent values. This strange behavior associated with the PMMA-grafted channel is attributed to the abovementioned issues with glassy PMMA and, in addition, a possible non-uniform grafted coating, which could lead to inhomogeneous wetting. A similar, albeit weaker effect is observed with the titled channel (Fig. 7f).

### LAOS of PMMA quasi-monolayers with bicone and DWR geometries and comparison to the results from the ISR

In order to complete the assessment of the presence of the 2nd harmonics in interfacial rheology, we performed dynamic strain sweep measurements at  $25^\circ\text{C}$  at  $\omega = 0.1$  Hz, using the bicone geometry without active control of the surface pressure. A highly concentrated layer was spread to get sufficient torque signal. The related magnitude spectrum of the Fourier transform of the excitation signal is shown in Fig. 8a for strain amplitude of  $\gamma_0 = 1\%$ . This signal has a typical signal-to-noise (S/N) ratio of 1000:1 for the first harmonic. Interestingly, over the entire investigated range of strain amplitudes, no even harmonics are present, but they could be hidden under the shoulder of the fundamental peak. The resolution of the experiment is not high enough to differentiate these peaks. In comparison with the ISR, the bicone geometry is more robust with respect to torque resolution and the deformation, with no defects and asymmetries in the setup and the interfacial tool.

Similar results are obtained for the DWR geometry by performing dynamic strain sweep measurements, again at  $25^\circ\text{C}$  and  $\omega = 0.1$  Hz. The quasi-monolayer was created in a

**Fig. 7** FT magnitude spectra of PMMA quasi-monolayer using the ISR with (a) Teflon-coated needle,  $\lambda = 18$  and surface pressure 16 mN/m; (b) Teflon-coated needle,  $\lambda = 14$  and surface pressure 14 mN/m; (c) Teflon-coated needle with water/glycerol subphase,  $\lambda = 14$  and surface pressure 16 mN/m; (d) PMMA-grafted channel with Teflon-coated needle,  $\lambda = 14$  and surface pressure 12 mN/m; (e) PMMA-grafted glass capillary rod,  $\lambda = 18$  and surface pressure 12 mN/m; and (f) tilted channel (with Teflon-coated steel rod,  $\lambda = 14$ ) at strain amplitude of  $\gamma_0 = 1\%$  and surface pressure 16 mN/m. Insets: normalized amplitudes of the 2nd harmonics of PMMA as a function of strain amplitude. The excitation frequency was  $\omega = 0.1$  Hz. In (g), the lower panel the phases of the 2nd harmonic versus strain amplitude with different configurations: channel with Teflon-coated rod and  $\lambda = 18$  (filled circles); channel with Teflon-coated rod and  $\lambda = 14$  (filled squares); PMMA-grafted rod (open squares); PMMA-grafted channel and Teflon-coated rod (open circles); Teflon-coated rod in water/glycerol subphase (filled triangles) or tilted channel (open triangles)

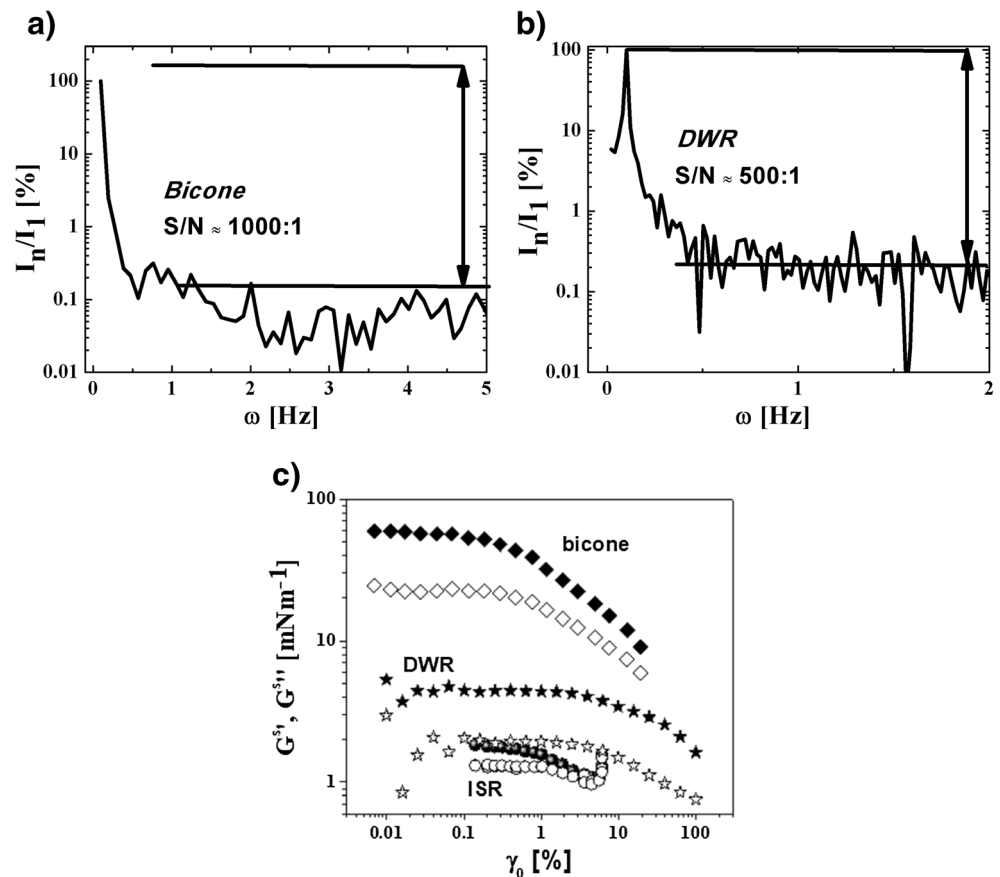


Langmuir trough where the control of the surface pressure was feasible using a Wilhelmy plate made by paper. Using the DWR, we obtained similar results with the bicone fixture with no clear even harmonics throughout the entire investigated range of strain amplitudes (Fig. 8b). Also, in the DWR setup, the second harmonic might be hidden under the (broad) fundamental peak. At the frequency of the 2nd harmonics, the peak of the fundamental shows as a shoulder. The third and the fourth harmonics are clearly detectable. This signal has a typical S/N ratio of 500:1 for the first harmonic ( $\gamma_0 = 1\%$ ). By design, the DWR fixture is also placed with high precision in

the shear gap and thus flow field asymmetries related to the measuring tools can be neglected.

In Fig. 8c, the dynamic strain sweep measurements using the bicone fixture, the DWR and the ISR (with Teflon-coated steel and  $\lambda = 18$ ) at  $\omega = 0.1$  Hz are presented. Comparing the interfacial moduli measured using the bicone fixture and the ISR, we note a huge difference (about two orders of magnitude) for both  $G^{sr}$  and  $G^{sn}$ . This is due to the fact that the two measurements were performed at different spreading concentrations (ISR:  $0.47 \text{ mg/m}^2$ ; bicone fixture:  $146.27 \text{ mg/m}^2$ ; DWR:  $5 \text{ mg/m}^2$ ). These huge differences in the polymer layer were

**Fig. 8** FT magnitude spectra of PMMA using (a) the bicone geometry and (b) the DWR geometry at strain amplitude of  $\gamma_0 = 1\%$  and excitation frequency of  $\omega_1 = 0.1$  Hz and surface pressure 16 mN/m. In (c), the oscillatory strain sweep data of ISR with  $\lambda = 18$  (circles), bicone (diamonds), and DWR (stars) are shown for  $\omega = 0.1$  Hz. Filled symbols refer to interfacial storage modulus and open symbols to interfacial loss modulus. The surface concentration of PMMA for the measurement with the bicone is  $146.27 \text{ mg/m}^2$ , for the DWR measurement, it is  $5 \text{ mg/m}^2$  while for the ISR, it is  $0.47 \text{ mg/m}^2$



necessary in order to perform reliable measurements (given the reduced sensitivity of bicone and DWR compared to the ISR).

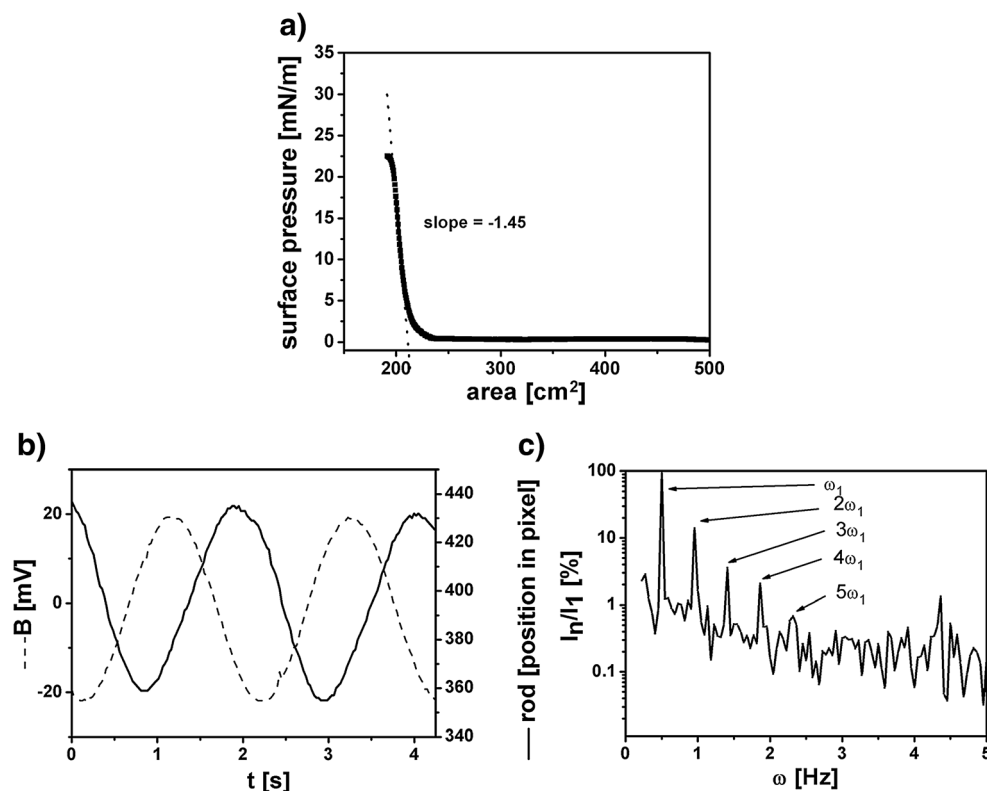
Subsequently, the results from the Fourier analysis of the measurement performed on the different surface shear setups will be compared. To be able to understand the differences detected in the three setups, the measurement parameters and conditions need to be discussed, as they have a direct effect on the resulting monolayer. Based on the three setups compared here, the ISR is the most sensitive technique and able to measure at the lowest surface pressure ( $0.47 \text{ mg/m}^2$ ). The material in the monolayer is less compressed when comparing it with the ISR ( $5 \text{ mg/m}^2$ ) or the DWR ( $146.27 \text{ mg/m}^2$ ). These different pressure values result in higher surface shear moduli (Fig. 8c). In the case of the bicone, a much higher surface concentration is used and the surface pressure might already create a layer that is at the crossover to a multilayer system.

The LAOS measurements using the ISR-setup show in the Fourier analysis higher harmonics (Fig. 7). These include, apart from the excitation peak, as a primary peak the second harmonic, but also the third and fourth are detected easily. When comparing these results of the different setups for measuring surface rheological properties, the ISR (Fig. 7), the DWR (Fig. 8b), and the bicone (Fig. 8a), the detected second harmonics are most clearly discernible in the ISR setup, and for the DWR and the bicone, the 2nd harmonics were not

present or hidden under the broad peak at the fundamental frequency; in any case, they should be weaker. The third and the fourth harmonic are clearly detectable.

As the even harmonics are present for both the asymmetric and symmetric channels, asymmetry in shape is not the main cause for even harmonics. Another possible origin of the second harmonics could be due to a non-uniform behavior of the monolayer upon shearing. Under the assumption that the magnetic rod is of a uniform shape, the rod would exert the same force in both directions on the interfacial layer. If the monolayer is uniform, even harmonics would not show. The monolayer has to contain some kind of inhomogeneities, so that the force acting upon the magnetic rod could result in a non-uniform movement. A tentative explanation to why this would be possible could be differences of the density of the monolayer, respectively, slight fluctuations in the surface pressure. To shed more light upon the behavior of the monolayer, experiments that examine the homogeneity of the monolayer are needed. Such could be doping the monolayer with tracer particles and then follow their behavior with, e.g., multiple particle tracking. Generally, creating monolayers in the Langmuir trough is a well-established method. As in the ISR, the surface pressure is quite low (here, corresponding to a surface concentration of  $0.47 \text{ mg/m}^2$ ), the inhomogeneities do not need to be very large to result in non-uniform movements. Such

**Fig. 9** PS-latex (550 nm diameter) quasi-monolayer at the air-water interface at 25 °C. Surface pressure versus area isotherm for an ethanol-washed sample (a). A set of time (b) and frequency (c) data are presented. The frequency data shows the FT of the rod position for the PS particle (550 nm) layer at a surface pressure of  $2 \text{ mN m}^{-1}$  (subphase pH = 5), a strain amplitude of  $\gamma_0 = 5\%$ , and an excitation frequency of 0.5 Hz



inhomogeneities might originate from the position of the magnetic rod inside the channel, like, e.g., one end closer to the end of the channel, and therefore, the rod is exposed to a slightly different curvature of the surface, resulting in a different local pressure.

### Colloidal (PS-latex) quasi-monolayers: FTR analysis of viscous interface with the ISR

**Surface pressure isotherms** Given the nonlinear rheological behavior in bulk systems of colloidal suspensions, layers of polystyrene (PS) latex particles appear to be promising candidates for investigating rheological nonlinearities at the water-air interface. The investigated PS latex particles with an average diameter of 538 nm (and a size dispersity below 5%) were synthesized according to the literature (Retsch et al. 2009) and spread as explained earlier (see section “Materials”). A surface pressure-area isotherm of the sample after ethanol washing and removal of the amphiphilic polymer fraction (which represents unavoidable contaminants from the preparation of the particles) in Fig. 9a shows one steep slope of  $-1.45 \text{ mN m}^{-1} \text{ cm}^{-2}$  for the layer compression, as generally observed for neat particle systems (Truzzolillo et al. 2016).

**Linear viscoelasticity** To determine the viscoelastic properties of the particle quasi-monolayer, rheological measurements on the ethanol-washed sample were performed at 25 °C and at a surface pressure of  $2 \text{ mN m}^{-1}$ . The corresponding low-strain

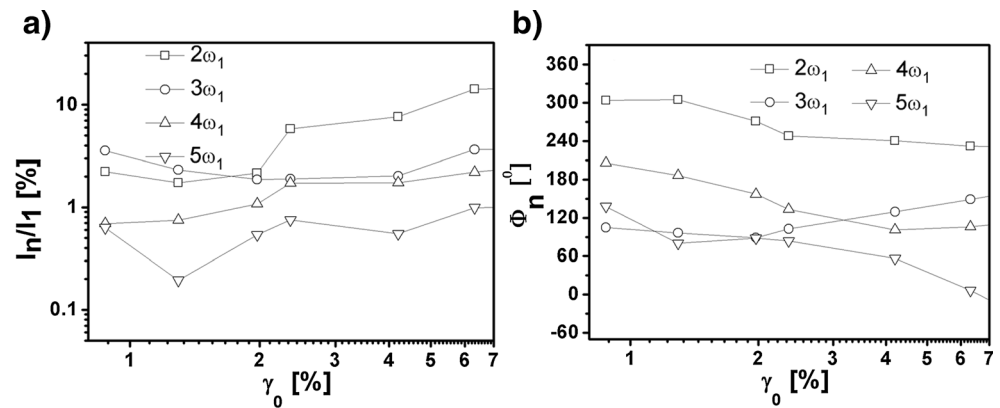
interfacial moduli could not be resolved; however, Fourier transform analysis could be performed at large deformations.

**FTR analysis** For these experiments, a surface pressure of  $2 \text{ mN m}^{-1}$  was chosen, since the layer should not be too stiff for the magnetic rod to easily move through the layer. Results from the LAOS experiments with the PS particle layer, under a strain amplitude  $\gamma_0 = 5\%$ , a frequency  $\omega = 0.5 \text{ Hz}$  and a subphase pH of 5, are summarized in Fig. 9b, c, where the time domain data and the magnitude spectra, respectively, are depicted. The magnitude spectrum shows higher harmonics up to the 5th harmonic (Fig. 9c). The intensity of the higher harmonics is decreasing with increasing frequency, in agreement with the respective behavior of bulk systems (Klein et al. 2007). A particularly interesting feature is the (reproducible) high intensities of the even harmonics, which were reported also above for the PMMA layer.

Figure 10 depicts the  $\gamma_0$ -dependent magnitudes and phases of the higher harmonics for the latex particle layer more clearly. The intensity for all observed harmonics increases slightly as a function of strain amplitude (Fig. 10a). When compared with bulk latex samples at much higher particle fraction, the present particle layer at the water-air interface exhibits larger intensity of the 2nd and the 4th harmonics (Klein 2005). Intuitively, one may expect that much larger strain amplitudes are needed in order to influence the interfacial particle arrangement due to the presence of lateral capillary and van der Waals forces between the particles. However, the linear



**Fig. 10** Nonlinear rheological data PS-latex quasi-monolayer at the water-air interface: magnitudes of harmonics (a) and phases (b). The measurements were performed at a subphase pH of 5 and a surface pressure of  $2 \text{ mN m}^{-1}$ . The excitation frequency was  $\omega = 0.5 \text{ Hz}$ . Note, the error is within the size of the symbols



response and the surface pressure isotherm of Fig. 9a indicate that the layer is rather weak, suggesting that electrostatic repulsions of the charged carboxyl functions (from the acrylic acid comonomer) dominate the particle-particle interactions (Truzzolillo et al. 2016). Harmonics higher than the 5th are not discernible for the particle layer due to the high noise level. In the phase information of Fig. 10b, the 2nd and the 3rd harmonics change only slightly their values at higher  $\gamma_0$ . This result indicates a stable and reproducible signal (Klein et al. 2007). Note that it has been possible to plot the data up to a strain amplitude of  $\gamma_0 = 6.3\%$  because at this amplitude, the nonlinearities of the subphase are still negligible, compared to the nonlinearities of the sample.

### Discussion of issues associated with measurements using the magnetic-rod ISR

As can be seen in Fig. 4, the PMMA layer exhibits a dominant elastic behavior. In the frequency sweep (Fig. 4a) utilizing the Teflon-coated steel magnetic rod, the moduli crossover occurs at angular frequency of 2 rad/s. Using the Teflon-coated steel magnetic rod, from the strain amplitude sweep (Fig. 4b), the sample response is elastic up to  $\gamma_0 = 5\%$ , and we can detect a linear regime up to  $\gamma_0 = 0.3\%$ . The time domain data of the previous dynamic strain sweep data were analyzed with FTR. For the PS latex layer, the linear viscoelastic response was too weak to determine the interfacial moduli. However, the nonlinear signal was sufficiently strong to perform a Fourier transform analysis.

With the help of FTR, the crossover from the linear to the nonlinear regime and the strain-dependent evolution of nonlinearities are detected in both polymer and PS-latex quasi-monolayers. Based on the experimental results presented above, the analysis of the setup and the rheological data allows to make general considerations about the resulting limitations and potential improvements of the implemented interfacial FTR technique. The underlying parameters can be divided

into three major categories: (a) rheology-specific parameters, (b) instrument-specific parameters, and (c) sample-specific parameters. The individual contributions are discussed in further detail below.

### Instrument-specific parameters

In order to perform FT rheological measurements from the linear to the nonlinear regime, it is necessary to be able to access a broad range of strain amplitudes and frequencies of the movement of the magnetic rod. To identify potential modification of the technical setup, which could extend the measuring range and improve the data quality and especially the sensitivity of the setup, the following three components need to be considered: (i) the magnetic field uniformity and enhanced strength of the magnetic field (which couples to the magnetic moment of the rod). This was recently achieved with a new design of the ISR using magnetic tweezers instead of Helmholtz coils (Tajuelo et al. 2015; Tajuelo et al. 2016), (ii) the magnetic rod and channel geometry (Reynaert et al. 2008), and (iii) the optical detection system (specifically the camera resolution, the field of view, and the image acquisition speed in frames per second).

The maximum force, which can be applied to the sample layer, depends on the magnetic coupling of the magnetic rod with the field of the Helmholtz coils. The Helmholtz coils and the driving power supplies of the commercial setup used are designed to provide the necessary magnetic field strength for the experiments with fluid samples. For very stiff samples like the highly compressed layers, the field strength or rod magnetization is not sufficient to move the magnetic rod. The magnetic rod and the channel geometry could be further improved, by further improving the symmetry and the channel length, as already discussed above in the results section and in earlier literature (Reynaert et al. 2008).

With respect to the optical system, the most relevant parameters are the camera resolution and the field of view. The minimum detectable excitation for the strain amplitude  $\gamma_0$  depends on the magnification of the camera lens. With a higher magnification, a smaller  $\gamma_0$  can be observed compared to the current

setup, for which the lower limit of  $\gamma_0$  was 0.1%. This is because a larger field of view was needed for larger strain amplitudes applied in subsequent measurements and it is not possible to change the camera resolution in a set of experiments for the same sample. This limitation also calls for a larger field of view to be able to accurately detect large rod displacements under identical experimental conditions. If at very large displacements, the end of the magnetic rod leaves the field of view, this data set cannot be interpreted correctly by FT analysis.

Another important factor of the camera is the acquisition speed. Detection of high frequencies is limited by the frame rate of the camera. As already discussed, the maximum detectable frequency is half the sampling frequency. The current frame rate of the camera (30 frames per second) imposes the limit of a maximum detectable frequency of 15 Hz, which represents a limitation for rheological excitation frequencies exceeding 1 Hz as one cannot detect a sufficient number of higher harmonics. To address this limitation, a camera with a frame rate about 20 to 50 times higher than the maximum excitation frequency would be desirable. This number originates from the lower detection limit of the 9th harmonic multiplied by a factor of 2 between the Nyquist frequency and the sampling rate.

### Sample-related issues

Suitable monolayer sample systems that can be investigated by FT-ISR for their nonlinear rheological behavior need to comply with the following three requirements: (i) sufficient fluidity or low stiffness of the sample layer, (ii) reversibility of the layer deformation, and (iii) sufficient sample-rod contact (to prevent slip during shear). The surface pressure is an additional, externally controllable parameter, which sets the layer stiffness. With the used setup and magnetic field, the latex layer studied exhibits the needed fluidity to be investigated by FT-ISR only at small surface pressures (or large surface areas). The glassy PMMA layer is microscopically heterogeneous and is also appropriate for FT-ISR at relatively low surface pressures (see section “Polymeric quasi-monolayers: Surface pressure isotherms, linear viscoelasticity and FTR analysis with the ISR”). In addition, a strong adhesive contact between the sample layer and the shearing rod is necessary to prevent slip at the sample-rod contact. Typically, the magnetic steel rod is coated with a low surface energy material (Teflon) to ensure floating at the air-water interface. This coating has the adverse effect of providing only a weak interaction with the sample material, but changing to a high surface energy coating would require a substantial redesign of the rod. The present rod is made of stainless steel and consequently has a higher density than the water subphase. The rod is kept at the air-water interface solely by the water surface tension. When changing to a more polar rod coating the density of the rod density has to be reduced below the water density to keep the rod floating by buoyancy. Such designs are the basis of the employed glass capillary rod

described above and are currently under investigation by other groups utilizing hollow tubes partially filled with a magnetizable material (Reynaert et al. 2008).

### Summary and conclusions

In this work, we have implemented Fourier transform rheology (FTR) in the magnetic-rod interfacial stress rheometer (ISR) in order to explore the possibility of measuring the nonlinear rheological properties of fluid interfaces with this arrangement. We used Langmuir layers from linear polymers (PMMA) or colloidal (PS-latex) particles at the air-water interface. PMMA formed an elastic albeit heterogeneous glassy layer, since despite plasticization due to water sorption, its glass transition temperature remained high. On the other hand, PS latex formed a viscous layer. We performed large amplitude oscillatory shear (LAOS) deformations. The excitation signal had a signal-to-noise ratio of about 1000:1 and the response signal could reach a signal-to-noise ratio of about 200:1. The reference pure water subphase did not exhibit any detectable mechanical nonlinearity up to strain amplitudes of 5%. The observed nonlinearities for strain values larger than 5% are measurement artifacts originating from a combination of factors, primarily the inhomogeneous surface geometry around the ends of the channel and the presence of flow asymmetries. The effects of surface tension in case of inhomogeneous wetting can also be a factor. The adaptation of the measurement and control software allows performing nonlinear FT rheological measurements at the air-water interface, including a user-defined oversampling mode to improve the signal-to-noise ratio.

The take-home message of this work is that extra caution is needed in interpreting the results when measuring LAOS with the magnetic-rod ISR. Of particular concern is the appearance of even harmonics. Such even harmonics might have their origin in the experimental setup, but also in material properties. To reach this conclusion, we used different methodologies and combinations of magnetic-rod and channel with the ISR, and complemented the investigation with measurements using the bicone and the double wall ring fixtures, both mounted on commercial rheometers. With the magnetic-rod ISR, we measured the nonlinear rheology of PMMA with channels of two different widths (aspect ratio of channel width to rod diameter  $\lambda = 14$  and 18). We prepared and tested magnetic, PMMA-grafted glass capillary rods, and further modified the channel by grafting it with PMMA. We also increased the bulk viscosity of the subphase 10 times using a mixture of glycerol/water in order to examine the effect of the subphase contribution. Finally, measurements were performed with a non-coaxial channel to study the effect of a highly asymmetric flow field in the channel to the intensity of the even harmonics. In all cases, the results with ISR indicated the presence of even harmonics whose amplitude increase with the strain amplitude. Notably, even harmonics were

not directly observed when using the bicone and the DWR fixtures, but when looking at the fundamental harmonic, the frequency resolution of the measurements is not sufficient to resolve the weak second harmonic. Especially in the DWR, a shoulder at the frequency of the second harmonic may be present. Moreover, for both the bicone and DWR setups, the ‘surface concentration’ of PMMA was much higher (at least one order of magnitude) compared to the ISR, due to sensitivity limits. Similar results were obtained with the ISR and a viscous layer prepared from an ethanol-washed PS-latex dispersion. Some of the abovementioned artifacts have an influence on the even harmonics. Additionally, the existence of the shoulder of the fundamental harmonic in the experimental results of the bicone and DWR setups may reflect the presence of a second harmonic, which is weaker compared to that in the ISR data. However, more work with different materials is needed to clarify this point.

With the field of LAOS in bulk systems evolving rapidly, alternative approaches to FTR, which can offer various advantages (Zang et al. 2010) could be applied also to 2D systems at the air-water interface. At the same time, further FT-ISR investigations could be extended to other polymer samples, such as poly (n-butyl acrylate) which has a low glass transition temperature. However, the present results suggest that even harmonics are unavoidable when measuring LAOS with the magnetic-rod ISR, but could also give important information about the monolayer examined. The present study can serve as a practical guide in this direction. Further research is needed to analyze the uniformity of the monolayer, such like multiple particle tracking. Despite the current progress, a remaining grand challenge is to reliably perform LAOS with the ISR rheometer, in order to expand its applicability, considering that it can resolve very low moduli and offers advantages such as relatively easy coupling with in situ structural probes (microscopy, light scattering).

**Acknowledgements** We thank Maria Kaliva for her help with grafting the glass rod and POM channel, and Nicolas Vogel and Markus Retsch for their help with the development of the particle purification procedure. We acknowledge Laurence de Viguierie for the help with the initial ISR measurements.

**Funding information** Partial support has been received by the European Commission (ITN “Comploids”, FP7-234810, and Horizon2020-INFRAIA-2016-1, EUSMI project no. 731019) and the Greek General Secretariat for Research and Technology (Heraclitos II program 2011).

**Publisher's note** Springer Nature remains neutral with regard to jurisdictional claims in published maps and institutional affiliations.

## References

Barman S, Christopher GF (2014) Simultaneous interfacial rheology and microstructure measurement of densely aggregated particle laden interfaces using a modified double wall ring interfacial rheometer. *Langmuir* 30(32):9752–9760

- Binks BP (2002) Particles as surfactants - similarities and differences. *Curr Opin Colloid Interface Sci* 7(1–2):21–41. [https://doi.org/10.1016/S1359-0294\(02\)00008-0](https://doi.org/10.1016/S1359-0294(02)00008-0)
- Binks B, Horozov TS (2006) Colloidal Particles at Liquid Interfaces. In: Cambridge Univ. Press, Cambridge
- Brooks CF (1999) An interfacial stress rheometer to study the shear rheology of Langmuir monolayers. Ph.D. thesis, Stanford University, USA. USA
- Brooks CF, Fuller GG, Frank CW, Robertson CR (1999) An interfacial stress rheometer to study rheological transitions in monolayers at the air-water interface. *Langmuir* 15(7):2450–2459. <https://doi.org/10.1021/la980465r>
- Cho KS, Hyun K, Ahn KH, Lee SJ (2005) A geometrical interpretation of large amplitude oscillatory shear response. *J Rheol* 49(3):747–758. <https://doi.org/10.1122/1.1895801>
- Choi SQ, Steltenkamp S, Zasadzinski JA, Squires TM (2011) Active microrheology and simultaneous visualization of sheared phospholipid monolayers. *Nat Commun* 2:312. <https://doi.org/10.1038/ncomms1321>
- Danov KD, Radulova GM, Kralchevsky PA, Golemanov K, Stoyanov SD (2012) Surface shear rheology of hydrophobin adsorption layers: laws of viscoelastic behaviour with applications to long-term foam stability. *Faraday Discuss* 158:195–221. <https://doi.org/10.1039/c2fd20017a>
- de Gennes P-G, Brochard-Wyart F, Quéré D (2004) Capillarity and wetting phenomena. Springer, NY
- de Viguierie L, Keller R, Jonas U, Berger R, Clark CG, Klein CO, Vlassopoulos D (2011) Effect of the molecular structure on the hierarchical self-assembly of Semifluorinated alkanes at the air/water Interface. *Langmuir* 27(14):8776–8786. <https://doi.org/10.1021/la201377f>
- Emi P, Parker A (2012) Nonlinear viscoelasticity and shear localization at complex fluid interfaces. *Langmuir* 28(20):7757–7767. <https://doi.org/10.1021/la301023k>
- Emi P, Fischer P, Windhab EJ, Kusnezov V, Stettin H, Lauger J (2003) Stress- and strain-controlled measurements of interfacial shear viscosity and viscoelasticity at liquid/liquid and gas/liquid interfaces. *Rev Sci Instrum* 74(11):4916–4924. <https://doi.org/10.1063/1.1614433>
- Emi P, Jerri HA, Wong K, Parker A (2012) Interfacial viscoelasticity controls buckling, wrinkling and arrest in emulsion drops undergoing mass transfer. *Soft Matter* 8(26):6958–6967. <https://doi.org/10.1039/c2sm25438g>
- Ewoldt RH, Bharadwaj NA (2013) Low-dimensional intrinsic material functions for nonlinear viscoelasticity. *Rheol Acta* 52(3):201–219. <https://doi.org/10.1007/s00397-013-0686-6>
- Fardin M, Perge C, Casanellas L, Hollis T, Taberlet N, Ortin J, Lerouge S, Manneville S (2014) Flow instabilities in large amplitude oscillatory shear: a cautionary tale. *Rheol Acta* 53(12):885–898. <https://doi.org/10.1007/s00397-014-0818-7>
- Fischer P, Emi P (2007) Emulsion drops in external flow fields - the role of liquid interfaces. *Curr Opin Colloid Interface Sci* 12(4–5):196–205. <https://doi.org/10.1016/j.cocis.2007.07.014>
- Fischer P, Brooks CF, Fuller GG, Ritcey AM, Xiao YF, Rahem T (2000) Phase behavior and flow properties of "hairy-rod" monolayers. *Langmuir* 16(2):726–734. <https://doi.org/10.1021/la990779u>
- Fitzgibbon S, Shaqfeh ESG, Fuller GG, Walker TW (2014) Scaling analysis and mathematical theory of the interfacial stress rheometer. *J Rheol* 58(4):999–1038
- Fujii Y, Nagamura T, Tanaka K (2010) Relaxation of poly (methyl methacrylate) at a water interface. *J Phys Chem B* 114:3457–3460. <https://doi.org/10.1021/jp909373g>
- Fuller GG (2003) Rheology of mobile interfaces. *Rheology Rev*:77–123
- Fuller GG, Vermant J (2011) Editorial: dynamics and rheology of complex fluid-fluid interfaces. *Soft Matter* 7(17):7583–7585. <https://doi.org/10.1039/c1sm90055b>



- Fuller GG, Vermant J (2012) Complex fluid-fluid interfaces: rheology and structure. In: J. M. Prausnitz. In: Annual review of chemical and biomolecular engineering, Vol 3, vol 3, pp 519–543
- Gordon TS (1986) The Stress Deformation Interfacial Rheometer. The University of Pennsylvania, Ph.D. thesis, USA
- Grenander U (1959) Probability and statistics: the Harald Cramér volume. Almqvist & Wiksell, Uppsala
- Hancock BC, Zografis G (1994) The relationship between the glass transition temperature and the water content of amorphous pharmaceutical solids. *Pharm Res* 11:471–477. <https://doi.org/10.1023/A:1018941810744>
- Hermans E, Vermant J (2014) Interfacial shear rheology of DPPC under physiologically relevant conditions. *Soft Matter* 10(1):175–186. <https://doi.org/10.1039/c3sm52091a>
- Hilles H, Monroy F, Bonales LJ, Ortega F, Rubio RG (2006) Fourier-transform rheology of polymer Langmuir monolayers: analysis of the non-linear and plastic behaviors. *Adv Colloid Interf Sci* 122(1–3):67–77. <https://doi.org/10.1016/j.cis.2006.06.013>
- Hollenbeck EC, Fong JCN, Lim JY, Yildiz FH, Fuller GG, Cegelski L (2014) Molecular determinants of mechanical properties of *V. cholerae* biofilms at the air-liquid interface. *Biophys J* 107(10):2245–2252. <https://doi.org/10.1016/j.bpj.2014.10.015>
- Hyun K, Wilhelm M (2009) Establishing a new mechanical nonlinear coefficient  $Q$  from FT-rheology: first investigation of entangled linear and comb polymer model systems. *Macromolecules* 42(1):411–422. <https://doi.org/10.1021/ma8017266>
- Hyun K, Wilhelm M, Klein CO, Cho KS, Nam JG, Ahn KH, McKinley GH (2011) A review of nonlinear oscillatory shear tests: analysis and application of large amplitude oscillatory shear (LAOS). *Prog Polym Sci* 36(12):1697–1753. <https://doi.org/10.1016/j.progpolymsci.2011.02.002>
- Israelachvili J (2011) Intermolecular and surface forces, 3rd edn. Elsevier, Amsterdam
- Jaensson N, Vermant J (2018) Tensiometry and rheology of complex interfaces. *Curr Opin Colloid Interface Sci* 37:136–150. [doi.org/10.1016/j.cocis.2018.09.005](https://doi.org/10.1016/j.cocis.2018.09.005)
- Jaishankar A, Sharma V, McKinley GH (2011) Interfacial viscoelasticity, yielding and creep ringing of globular protein-surfactant mixtures. *Soft Matter* 7(17):7623–7634. <https://doi.org/10.1039/c1sm05399j>
- Kim HC, Choi YH, Bu W, Meron M, Lin B, Won Y-Y (2017) Increased humidity can soften glassy Langmuir polymer films by two mechanisms: plasticization of the polymer material and suppression of the evaporation cooling effect. *Phys Chem Chem Phys* 19:10663–10675. <https://doi.org/10.1039/c7cp00785j>
- Klein C (2005) Rheology and Fourier-transform rheology on water-based systems. Ph.D. thesis, Mainz, Germany
- Klein CO, Spiess HW, Calin A, Balan C, Wilhelm M (2007) Separation of the nonlinear oscillatory response into a superposition of linear, strain hardening, strain softening, and wall slip response. *Macromolecules* 40(12):4250–4259. <https://doi.org/10.1021/ma062441u>
- Klein C, de Viguier L, Christopoulou C, Jonas U, Clark CG, Mullen K, Vlassopoulos D (2011) Viscoelasticity of semifluorinated alkanes at the air/water interface. *Soft Matter* 7(17):7737–7746. <https://doi.org/10.1039/c1sm05357d>
- Kotula AP, Anna SL (2015) Regular perturbation analysis of small amplitude oscillatory dilatation of an interface in a capillary pressure tensiometer. *J Rheol* 59:85–117. <https://doi.org/10.1122/1.4902546>
- Kralchevsky PA, Nagayama K (1994) Capillary forces between colloidal particles. *Langmuir* 10(1):23–36. <https://doi.org/10.1021/la00013a004>
- Krishnaswamy R, Majumdar S, Sood AK (2007) Nonlinear viscoelasticity of sorbitan tristearate monolayers at liquid/gas interface. *Langmuir* 23(26):12951–12958. <https://doi.org/10.1021/la701889v>
- Leal-Calderon F, Schmitt V (2008) Solid-stabilized emulsions. *Curr Opin Colloid Interface Sci* 13(4):217–227. <https://doi.org/10.1016/j.cocis.2007.09.005>
- Lopez JM, Hirta AH (2015) Coupling of the interfacial and bulk flow in knife-edge viscometers. *Phys Fluids* 27(4):042102
- Macosko CW, Guegan P, Khandpur AK, Nakayama A, Marechal P, Inoue T (1996) Compatibilizers for melt blending: premade block copolymers. *Macromolecules* 29(17):5590–5598. <https://doi.org/10.1021/ma9602482>
- Monteux C, Mangeret R, Laibe G, Freyssingas E, Bergeron V, Fuller G (2006) Shear surface rheology of poly(*N*-isopropylacrylamide) adsorbed layers at the air-water interface. *Macromolecules* 39(9):3408–3414. <https://doi.org/10.1021/ma052552d>
- Murray BS (2002) Interfacial rheology of food emulsifiers and proteins. *Curr Opin Colloid Interface Sci* 7(5–6):426–431. [https://doi.org/10.1016/s1359-0294\(02\)00077-8](https://doi.org/10.1016/s1359-0294(02)00077-8)
- Nagel M, Tervoort TA, Vermant J (2017) From drop-shape analysis to stress-fitting elastometry. *Adv Colloid Interf Sci* 247:33–51. <https://doi.org/10.1016/j.cis.2017.07.008>
- Pepicelli M, Verwijlen T, Tervoort TA, Vermant J (2017) Characterization and modelling of Langmuir interfaces with finite elasticity. *Soft Matter* 13(35):5977–5990
- Prucker O, Naumann CA, Ruhe J, Knoll W, Frank CW (1999) Photochemical attachment of polymer films to solid surfaces via monolayers of benzophenone derivatives. *J Am Chem Soc* 121(38):8766–8770. <https://doi.org/10.1021/ja990962+>
- Raghunandan A, Lopez JM, Hirta AH (2015) Bulk flow driven by a viscous monolayer. *J Fluid Mech* 785:283–300
- Reinheimer K, Grosso M, Wilhelm M (2011) Fourier transform rheology as a universal non-linear mechanical characterization of droplet size and interfacial tension of dilute monodisperse emulsions. *J Colloid Interface Sci* 360:818–825. <https://doi.org/10.1016/j.cis.2011.05.002>
- Retsch M, Zhou ZC, Rivera S, Kappl M, Zhao XS, Jonas U, Li Q (2009) Fabrication of large-area, transferable colloidal monolayers utilizing self-assembly at the air/water interface. *Macromol Chem Phys* 210(3–4):230–241. <https://doi.org/10.1002/macp.200800484>
- Reynaert S, Brooks CF, Moldenaers P, Vermant J, Fuller GG (2008) Analysis of the magnetic rod interfacial stress rheometer. *J Rheol* 52(1):261–285. <https://doi.org/10.1122/1.2798238>
- Rogers SA (2012) A sequence of physical processes determined and quantified in LAOS: an instantaneous local 2D/3D approach. *J Rheol* 56(5):1129–1151. <https://doi.org/10.1122/1.4726083>
- Rogers SA (2018) Large amplitude oscillatory shear: simple to describe, hard to interpret. *Phys Today* 71(7):34–40. <https://doi.org/10.1063/PT.3.3971>
- Rogers SA, Erwin BM, Vlassopoulos D, Cloitre M (2011) Oscillatory yielding of a colloidal star glass. *J Rheol* 55(4):733–752. <https://doi.org/10.1122/1.3579161>
- Rubinstein M, Colby RH (2003) Polymer physics. Oxford Univ. Press, NY
- Rühs PA, Scheuble N, Windhab EJ, Mezzenga R, Fischer P (2012) Simultaneous control of pH and ionic strength during interfacial rheology of beta-Lactoglobulin fibrils adsorbed at liquid/liquid interfaces. *Langmuir* 28(34):12536–12543. <https://doi.org/10.1021/la3026705>
- Rühs PA, Affolter C, Windhab EJ, Fischer P (2013a) Shear and dilatational linear and nonlinear subphase controlled interfacial rheology of beta-lactoglobulin fibrils and their derivatives. *J Rheol* 57(3):1003–1022. <https://doi.org/10.1122/1.4802051>
- Rühs PA, Boni L, Fuller GG, Inglis RF, Fischer P (2013b) In-situ quantification of the interfacial rheological response of bacterial biofilms to environmental stimuli. *PLoS One* 8(11):e78524. <https://doi.org/10.1371/journal.pone.0078524>
- Russel WB, Saville DA, Schowalter WR (1989) Colloidal dispersion. Cambridge Univ. Press, NY



- Sagis LMC (2011) Dynamic properties of interfaces in soft matter: experiments and theory. *Rev Mod Phys* 83(4):1367–1403. <https://doi.org/10.1103/RevModPhys.83.1367>
- Sagis LMC, Fischer P (2014) Nonlinear rheology of complex fluid-fluid interfaces. *Curr Opin Colloid Interface Sci* 19(6):520–529. <https://doi.org/10.1016/j.cocis.2014.09.003>
- Samaniuk JR, Vermant J (2014) Micro and macrorheology at fluid-fluid interfaces. *Soft Matter* 10(36):7023–7033. <https://doi.org/10.1039/c4sm00646a>
- Singh PK, Piyush K, Soulages JM, Ewoldt R, shear H F-s m-a o (2018) MAOS. *J Rheol* 62:277–293. <https://doi.org/10.1122/1.4999795>
- Srivastava S, Leiske D, Basu JK, Fuller GG (2011) Interfacial shear rheology of highly confined glassy polymers. *Soft Matter* 7(5):1994–2000. <https://doi.org/10.1039/c0sm00839g>
- Stocco A, Rio E, Binks BP, Langevin D (2011) Aqueous foams stabilized solely by particles. *Soft Matter* 7(4):1260–1267. <https://doi.org/10.1039/c0sm01290d>
- Tajuelo J, Pastor JM, Martinez-Pedrero F, Vazquez M, Ortega F, Rubio RG, Rubio MA (2015) Magnetic microwire probes for the magnetic rod interfacial stress rheometer. *Langmuir* 31(4):1410–1420. <https://doi.org/10.1021/la5038316>
- Tajuelo J, Pastor JM, Rubio MA (2016) A magnetic rod interfacial shear rheometer driven by a mobile magnetic trap. *J Rheol* 60(6):1095–1113. <https://doi.org/10.1122/1.4958668>
- Tajuelo J, Rubio MA, Pastor JM (2018) Flow field based data processing for the oscillating conical bob interfacial shear rheometer. *J Rheol* 62(1):295–311
- Theodoratou A, Jonas U, Loppinet B, Geue T, Stangenberg R, Keller R, Li D, Berger R, Vermant J, Vlassopoulos D (2016) Semifluorinated alkanes at the air-water Interface: tailoring structure and rheology at the molecular scale. *Langmuir* 32(13):3139–3151. <https://doi.org/10.1021/acs.langmuir.5b04744>
- Thijssen JHJ, Vermant J (2018) Interfacial rheology of model particles at liquid interfaces and its relation to (bicontinuous) Pickering emulsions. *Journal of Physics-Condensed Matter* 30(2):023002. <https://doi.org/10.1088/1361-648X/aa9c74>
- Torcello-Gomez A, Maldonado-Valderrama J, Galvez-Ruiz MJ, Martin-Rodriguez A, Cabrerizo-Vilchez MA, de Vicente J (2011) Surface rheology of sorbitan tristearate and beta-lactoglobulin: shear and dilatational behavior. *J Non-Newtonian Fluid Mech* 166(12–13):713–722. <https://doi.org/10.1016/j.jnnfm.2011.03.008>
- Truzzolillo D, Sharaf H, Jonas U, Loppinet B, Vlassopoulos D (2016) Tuning the structure and rheology of polystyrene particles at the air-water Interface by varying the pH. *Langmuir* 32(27):6956–6966. <https://doi.org/10.1021/acs.langmuir.6b01969>
- Underhill PT, Hirsra AH, Lopez JM (2017) Modelling steady shear flows of Newtonian liquids with non-Newtonian interfaces. *J Fluid Mech* 814:5–23
- van den Berg MEH, Kuster S, Windhab EJ, Sagis LMC, Fischer P (2018) Nonlinear shear and dilatational rheology of viscoelastic interfacial layers of cellulose nanocrystals. *Phys. Fluids* 30:072103
- van Dusschoten D, Wilhelm M (2001) Increased torque transducer sensitivity via oversampling. *Rheol Acta* 40(4):395–399. <https://doi.org/10.1007/s003970000158>
- Vandebriel S, Franck A, Fuller GG, Moldenaers P, Vermant J (2010) A double wall-ring geometry for interfacial shear rheometry. *Rheol Acta* 49(2):131–144. <https://doi.org/10.1007/s00397-009-0407-3>
- Vermant J, Vandebriel S, Dewitte C, Moldenaers P (2008) Particle-stabilized polymer blends. *Rheol Acta* 47(7):835–839. <https://doi.org/10.1007/s00397-008-0285-0>
- Verwijlen T, Moldenaers P, Stone HA, Vermant J (2011) Study of the flow field in the magnetic rod interfacial stress rheometer. *Langmuir* 27(15):9345–9358. <https://doi.org/10.1021/la201109u>
- Wilhelm M (2002) Fourier-transform rheology. *Macromol Mater Eng* 287(2):83–105. [https://doi.org/10.1002/1439-2054\(20020201\)287:2<83](https://doi.org/10.1002/1439-2054(20020201)287:2<83)
- Wilhelm M, Maring D, Spiess H (1998) Fourier-transform rheology. *Rheol Acta* 37:399–405. <https://doi.org/10.1007/s003970050126>
- Wilhelm M, Reinheimer K, Kubel J (2012) Optimizing the sensitivity of FT-rheology to quantify and differentiate for the first time the non-linear mechanical response of dispersed beer foams of light and dark beer. *Z Phys Chem* 226(7–8):547–567. <https://doi.org/10.1524/zpch.2012.0247>
- Witte KN, Kewalramani S, Kuzmenko I, Sun W, Fukuto M, Won Y-Y (2010) Formation and collapse of single-monomer-thick monolayers of poly(n-butyl acrylate) at the air-water Interface. *Macromolecules* 43:2990–3003. <https://doi.org/10.1021/ma901842q>
- Witten TA (2004) Structured fluids. Paper presented at the Oxford Univ. Press, NY
- Wu C, Lim JY, Fuller GG, Cegelski L (2012) Quantitative analysis of amyloid-integrated biofilms formed by Uropathogenic *Escherichia coli* at the air-liquid Interface. *Biophys J* 103(3):464–471. <https://doi.org/10.1016/j.bpj.2012.06.049>
- Xu H, Lask M, Kirkwood J, Fuller G (2007) Particle bridging between oil and water interfaces. *Langmuir* 23(9):4837–4841. <https://doi.org/10.1021/la063593i>
- Zang DY, Langevin D, Binks BP, Wei BB (2010) Shearing particle monolayers: strain-rate frequency superposition. *Phys Rev E* 81(1). <https://doi.org/10.1103/PhysRevE.81.011604>